A NOVEL FORM FINDING METHOD FOR FABRIC FORMWORK FOR CONCRETE SHELLS

Tom Van Mele, Philippe Block

Post-doctoral Researcher, ETH Zurich, Inst. of Technology in Architecture, Zurich, Switzerland, van.mele@arch.ethz.ch
Assistant Professor, ETH Zurich, Inst. of Technology in Architecture, Zurich, Switzerland, block@arch.ethz.ch

ABSTRACT

This paper introduces a new form finding approach for the design of flexible formwork, consisting of pre-stressed structural membranes, for the construction of thin, anticlastic, concrete shells. The approach is based on the Force Density Method and an adaptation of the nonlinear extension of Thrust Network Analysis (TNA). First, the adaptation of the basic version of TNA to tension-only structures is discussed, and fundamental assumptions are formulated. Key aspects herein are the use of reciprocal diagrams and the control of forces in indeterminate networks. Then, the strategy using an overall optimization process, for finding the closest possible tension-only, equilibrium surface to a given target surface under the appropriate loading (i.e. weight of the concrete) is presented. Finally, the strategy is applied to a chosen target surface and loads, and the equilibrium solutions for different starting points of the optimization process are discussed.

Keywords: *Concrete shells, pre-stressed membrane formwork, form finding, Force Density Method, Thrust Network Approach.*

1. INTRODUCTION

1.1 Concrete Shells

Concrete shells are efficient structures for medium to large-span space enclosures. When appropriately shaped, these structures carry loads through membrane action (i.e. axial force-only) rather than bending, which allow them to be thin, light, and elegant.

There are two key aspects in the realization of thin concrete shells: 1) the determination of an appropriate shape (through a form finding process), and 2) the actual construction. Regardless of the form finding method used to determine their shape, concrete shells typically have been constructed using rigid formwork, onto which wet concrete is poured or sprayed. The variety of shell shapes that can be constructed and especially the curvature that can be achieved is limited by the shape flexibility of this formwork.

Felix Candela, for example, limited all his concrete shell designs to shapes which could be derived from (a combination of) hyperbolic paraboloids (hypars), since these can be realized with a formwork consisting of only straight elements, simplifying the formwork drastically and allowing reuse for other applications (Fig. 1) [1].
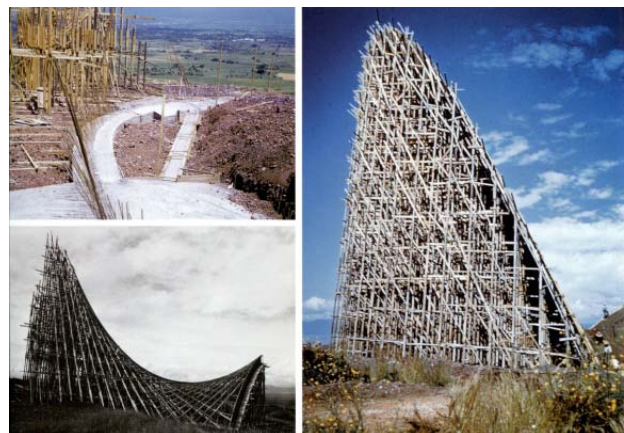
Figure 1*. Chapel Lomas de Cuernavaca [1]. The shape of the shell is derived from hyperbolic paraboloids, allowing the formwork to be constructed using straight elements.*

In any case, the construction of formwork is costly, time-consuming, and produces a huge amount of building waste, which are some of the reasons why concrete shells are no longer used as structural systems. Flexible formwork systems, however, using tensioned membrane structures, seem to address many of the challenges of typical shell construction and open new possibilities for shell design [2]. Furthermore, as it is well known that very slight improvements to the geometry of a shell can drastically improve its properties [3,4], the use of "flexible" formwork, i.e. formwork allowing more accurate shape control, could also increase a shell's structural performance.

1.2 Flexible Formwork

Fabric formwork for reinforced concrete construction is an emerging technology with the capacity to transform concrete architecture and reinforced concrete structures [5,6]. Currently, such formwork systems are used, primarily, to create beams, trusses, panels, simple, hanging vaults, slabs, and columns with expressive, natural curvature [6].

Figure 2. left) Fabric formwork for a beam with expressive, natural curvature, and right) simple vault cast on fabric formwork [5].

The work on vaults conducted at CAST, one of the leading labs in the development of fabric formwork [5], focuses on pre-cast and cast-in-place vaults that are formed with full-scale hanging fabric moulds using powerful industrial fabrics (Fig. 2) – essentially scaling- up Isler's model-making method into full-sized shell moulds.

In this paper, we will discuss a different approach, using structural pre-stressed formwork for the construction of thin, anticlastic, concrete shells; and introduce a new computational form finding approach for designing such formwork systems.

Given the shape of an anticlastic shell design, the objective of the presented method is to find the shape of the pre-stressed membrane surface (or cable network) that, under the weight of (wet) concrete, has the exact shape of the final shell. This allows concrete to be sprayed onto the membrane surface that then supports the (wet) concrete in the correct shape until it has hardened, after which the shell can stand on its own and the membrane formwork can be removed.

The approach is based on the Force Density Method [7,8] and an adaptation of the nonlinear extension of Thrust Network Analysis [9,10].

1.3 Force Density Method

The Force Density Method (FDM) is one of the main approaches for the form finding of tension structures, introduced by Linkwitz and Schek [7] for finding the equilibrium shape of tension networks. By introducing force densities, which are defined as the ratio of the axial force of a branch to its length, the equations expressing the equilibrium of the networks could be linearised. Due to the development of sparse matrix techniques, these linear equations could be solved efficiently.

Initial values for these force densities need to be chosen for the first-order form finding. To comply with additional conditions imposed to refine the design, the final equilibrium values of the force densities are then found in an iterative optimization process. The relations between the choice of force densities and the three-dimensional equilibrium solution are thus not straightforward. Furthermore, the method as discussed in [8], does not provide an optimization strategy for finding the appropriate distribution of force densities (and consequently of forces) to obtain a desired, specific three-dimensional shape.

1.4 Thrust Network Approach

Thrust Network Analysis (TNA) is a new methodology for generating vaulted compression-only networks and surfaces, with a similar framework as the Force Density Method [9,10]. Using reciprocal force diagrams [11], TNA provides a graphical and intuitive method, adopting the same advantages as graphic statics but offering a viable extension to fully three-dimensional problems. Reciprocal figures are introduced to

relate the geometry of the three-dimensional equilibrium networks to their internal forces. They allow the linearization of the equilibrium constraints and the control of the high level of indeterminacy of fully three-dimensional funicular networks.

In [10], a nonlinear extension of the basic TNA method is discussed that includes the degrees of indeterminacy of a three-dimensional network with arbitrary topology in an overall optimization set-up. Such a set-up opens up possibilities for making structurally informed design decisions in order to find the closest funicular network to an arbitrary input surface.

2. TNA FOR TENSION STRUCTURES

The TNA method is geared towards the design of funicular, i.e. compression-only, vaults and shells, but could of course also be used for the dual problem of tension-only networks

Applying TNA to tension-only membrane structures, demands a slight re-formulation of its assumptions:

- the structural action of the membrane is represented by a discrete network of forces with the external loads applied at the vertices;

- the force branches meet at nodes, which are in equilibrium with external forces applied to the nodes;

- the branches must all have axial tension forces only;

- all applied loads need to be vertical; and

- the nodes are only allowed to move vertically during the form-finding process.

The assumption about vertical loads seems strong and very restricting. It is, however, a reasonable assumption to make, considering that the membrane will only be used to support the (wet) concrete in a specific shape until it has hardened and can stand on its own, hence carrying only vertical gravity loads. Note that any tangential loads due to sliding of the wet concrete are ignored.

This section will explain how the underlying principles of the TNA framework can be used to achieve the goals of this project. Key aspects are the use of reciprocal diagrams and the control of the indeterminacy of networks with a higher valency than three, i.e. with more than three branches coming together at every node of the network.

2.1 Reciprocal Diagrams

The use of discrete force networks in combination with reciprocal force diagrams allows to determine and represent possible distributions of internal forces in a visual and intuitive manner.
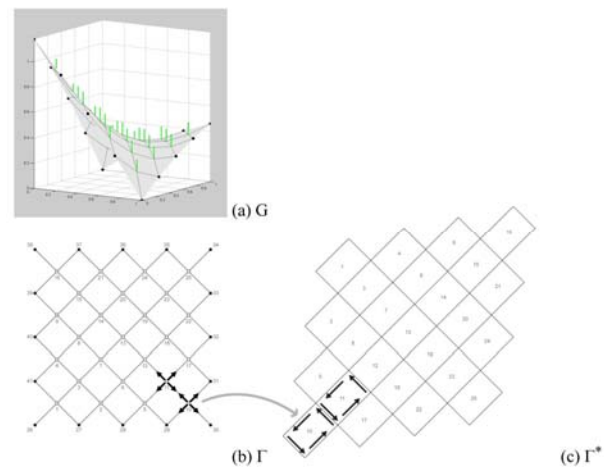
Figure 3. a) 3D network G in equilibrium with loads applied to its nodes; b) the primal grid Γ, which is the horizontal projection of G; and c) the dual grid Γ^*, which is the reciprocal of Γ and represents the equilibrium of horizontal force components in the system G.

Reciprocal diagrams are geometrically related such that corresponding branches are parallel, and branches which come together in a node in one of the diagrams form a closed polygon in the other, and vice versa (Fig. 3b-c). This geometrical relationship has an important structural interpretation: the closed polygons of the reciprocal diagram represent the static equilibrium of the nodes in the original diagram; and the lengths of the branches in the reciprocal are proportional to the axial forces along the corresponding branches in the original [9].

The grid in Figure 3b depicts the horizontal projection of a 3D network G at equilibrium with loads applied to its nodes (Fig. 3a). In TNA, this projection is called the primal grid, Γ.

The static in-plane equilibrium of Γ is represented by its closed reciprocal diagram, the dual grid Γ^*

(Fig. 3c). Note that all loads applied to *G* vanish in *Γ*, because they are perpendicular to the plane of *Γ*. Therefore, *Γ** represents and visualizes the equilibrium of all horizontal force components in the system *G*. We know that from such grids a tension-only solution is obtained if all faces in the dual grid are convex [12] and constructed by going around each corresponding node of the primal grid in a counter-clockwise direction [13], as illustrated in Figures 3b and 3c.

The solving strategy presented in this paper is largely based on the direct link between the force densities of FDM and the reciprocal diagrams of TNA. The force density of a branch in the network is defined as the ratio between the (axial) force in that branch, *s*, and its length, *l*. This ratio, and hence the value of the branch's force density, is also equal to the ratio between the horizontal component of the branch force, s_H, which is the length of the corresponding branch in the dual grid, l_H^*, and the horizontal component of the branch's length, l_H, which is the length of the branch in the primal grid. We thus have that

$$q = \frac{s}{l} = \frac{s_H}{l_H} = \frac{l_H^*}{l_H} \qquad (1)$$

As in FDM, TNA uses branch-node matrices to describe the topology of both grids. For detailed information on the construction of primal and dual grids and their respective branch-node matrices, the reader is referred to [10].

2.2 Indeterminate Networks

For typical network topologies used for the form finding of tension structures, the network *G* (and its planar projection *Γ*) have nodes with a valency of four (or higher), which means that they are statically indeterminate and have several possible internal force distributions. This means that different states of self-stress exist with different distributions of internal forces of *Γ* and corresponding 3D geometry.

Figure 4c shows a different dual grid for the primal grid of Figure 3, representing a different distribution of internal forces and therefore a different 3D solution in equilibrium with the applied loads (Fig. 4a). In this solution, more force is attracted by the highlighted sets of branches, each forming a continuous line through the network.
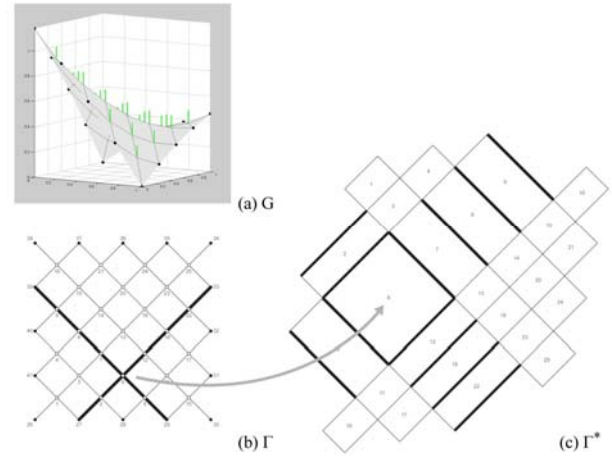
***Figure 4**. c) A different dual grid Γ* for the same primal grid Γ as in Figure 3b, representing a different distribution of internal forces and therefore a different 3D solution G in equilibrium with the loads, as shown in (a). Forces have been attracted along the highlighted cables in (b), as represented by the longer lengths in (c).*

In the 3D network, we can clearly see that this results in shallower curvature along those lines.

In the TNA framework, the x- and y-coordinates of the nodes are kept constant during the form finding process. Because of this constraint, the manipulations of the dual grid cannot be random; only variations which respect the reciprocal rules (see Section 2.1), are allowed. In [10], a rule is introduced which allows to determine the total number of degrees of freedom (DOF) *k* of the dual *Γ**, by inspection of the primal grid *Γ* alone:

$$k = 2f - m + c - 2 \qquad (2)$$

with *f* the number of faces in the primal grid, *m* the number of branches, and *c* the number of "closed loops".

The number of DOFs *k* (with *k < m*) equals the number of independent dual branches, i.e. the branches whose lengths can be chosen freely. The other branches are not independent, meaning that their lengths cannot be chosen. This represents the reciprocity constraint. Because of the link between the force densities and the reciprocal diagram (Eq. 1), this understanding of the DOF of the distribution of the forces on the primal grid, as represented in the dual grid, can be used to understand the DOF of the distribution of the force densities of possible tension networks in equilibrium with the applied loads.

For a quadrilateral grid, as used in Figures 3 and 4, it is clear that k equals the number of continuous lines of branches in the primal grid. This means that per continuous set, the force densities of the branches are dependent. Applying the rule given in Equation (2), k indeed counts as 2x40-64+0-2 = 14 for the networks of Figures 3 and 4. The identification of possible sets of branches for which the force densities can be chosen independently has been generalized to any topology in [14].

This insight provided by the TNA framework allows the straightforward description of the relation between the (k x 1) vector of independent, or free, force densities, b, and the (m x 1) vector of individual force densities of all branches, q, represented by an (m x k) matrix K:

$$q = K \cdot b \qquad (3)$$

3. APPROACHING A TARGET SURFACE

From the previous section, it is clear that the force distribution in a network can be controlled or "tweaked" to find a specific 3D geometry, i.e. the shape of the concrete shell that has to be built. For simple projects, it might be possible to do this manually, but when a solution needs to be found approximating a target surface in more sophisticated problems, this quickly becomes too tedious and an overall optimization process needs to be employed to find the desired distribution. The main challenge is to relate a change in the distribution of internal forces, or force densities, to the improvement of the approximation of the target surface. This process will be described next.

3.1 Problem Description

Given a target surface, represented by a 4-valent discrete network of branches and nodes, and a set of vertical external loads applied at the nodes, the tension-only solution needs to be found that is the best possible approximation of the target.

The target network is projected onto the plane to find the primal grid Γ, and from Γ a possible dual Γ^* is constructed. Equation (2) gives us k DOFs of Γ^*, the number of independent parameters that control the equilibrium and geometry of the 3D solution G. In section 2.2, it was shown that these are the continuous lines in the primal grid.

Then the values for the independent parameters, the "free" force densities b, should be found that minimize the vertical distance between the nodes of G and those of the target surface. This can be formulated as a least squares problem

$$\min_z \left\| z - z^T \right\|_2^2$$
$$\text{such that} \quad z = D^{-1}(p_z - D_f z_f) \qquad (4)$$

The constraints on the vertical position of the nodes immediately follow from the nodal equilibrium of the network, with p_z the applied vertical loads, z_f the z-coordinates of the boundary nodes, and $D = C^t Q C$ and $D_f = C^t Q C_f$, as described in [8]. It is sufficient to only consider the vertical equilibrium of the nodes, as their horizontal equilibrium is guaranteed by the closed reciprocal force diagram [9].

Such a least squares problem can be solved efficiently using the Levenberg-Marquardt Algorithm (LMA).

3.2 Solving Procedure

LMA is an iterative, hybrid, descent method that switches between the Steepest Descent Method (SDM) and the Gauss-Newton Method (GNM), based on a so-called *gain ratio* (see Eq. 9). For details on the method, the reader is referred to [15-17]. Here, we will give a brief description. For a given objective function $F(x)$, with

$$F(x) = \sum_{i=1}^m (f_i(x))^2 \qquad (5)$$

and from a starting point $x^{(0)}$, the method produces a series of vectors $x^{(1)}$, $x^{(2)}$, … that converges to x^*, a local minimiser of F.

Essentially, each iteration consists of finding (i) a descent direction, and (ii) a step length giving a good decrease in F-value. The step h is found as the local minimiser of a linear model of the objective function, L, by solving the following problem:

$$\left(J^t(x)J(x) + \mu I\right)h = -J^t(x)f(x)$$
$$\text{with} \quad \mu \geq 0 \qquad (6)$$

with $f(x)$ the value of the objective function at the previous iteration, $J(x)$ the Jacobian matrix of $f(x)$, I an identity matrix, and μ a damping factor.

Note that Equation (6) is a damped version of the GNM approach for finding $\boldsymbol{h}$. The damping parameter μ influences both the direction and the size of the step in several ways: (i) for all $\mu > 0$, the coefficient matrix is positive definite, and this ensures that $\boldsymbol{h}$ is a descent direction; (ii) for large values of μ, we get a short step in the SDM direction, which is good if the current iterate is far from the solution; and (iii) if μ is very small, the step is approximately the GNM step, which is good when the current iterate is close to the final solution. The initial μ-value is

$$\mu^{(0)} = \tau \cdot \max_i \left\{ a_{ii}^{(0)} \right\}$$
$$\text{with} \quad \boldsymbol{A}^{(0)} = \boldsymbol{J}(\boldsymbol{x}^{(0)})^t \boldsymbol{J}(\boldsymbol{x}^{(0)}) \qquad (7)$$

with τ chosen by the user. During the iteration process, μ is updated based on the *gain ratio ρ*, which is defined as the ratio between the actual gain in $\boldsymbol{F}$ and the gain predicted by the linear model $\boldsymbol{L}$ [17].

$$\rho = \frac{F(\boldsymbol{x}) - F(\boldsymbol{x} + \boldsymbol{h})}{L(0) - L(\boldsymbol{h})} \qquad (8)$$

A large value of ρ indicates that the linear model is good approximation of the actual cost function, and we can decrease μ so that the next LMA step is closer to the GNM step. If ρ is small, then the linear model is a poor approximation, and we should increase μ with the aim of getting closer to the SDM direction and reducing the step length. The iterative procedure is stopped if one of the following criteria is met [17]:

$$\left\| \boldsymbol{J}(\boldsymbol{x})^t \boldsymbol{f}(\boldsymbol{x}) \right\|_\infty \leq \varepsilon_1$$
$$\left\| \boldsymbol{x}_{new} - \boldsymbol{x} \right\| \leq \varepsilon_2 \left(\left\| \boldsymbol{x} \right\| + \varepsilon_2 \right) \qquad (9)$$
$$k \geq k_{\max}$$

with ε_1, ε_2, and k_{max} chosen by the user.

3.3 Jacobian Matrix

The Jacobian matrix can be derived in a similar fashion as described in Schek [8]. The additional conditions imposed on the system are function of the *z*-coordinates of the nodes, which in turn are function of the force densities, $\boldsymbol{q}$, and those are function of the independent parameters, $\boldsymbol{b}$. Therefore, the additional conditions can be reformulated as a function of the independent parameters $\boldsymbol{b}$.

$$\boldsymbol{f}^*(\boldsymbol{b}) = \boldsymbol{f}(\boldsymbol{z}(\boldsymbol{q}(\boldsymbol{b}))) = \boldsymbol{z} - \boldsymbol{z}^T = 0 \qquad (10)$$

The Jacobian, $\boldsymbol{J(b)}$, relating a change in the independent parameters $\boldsymbol{b}$ to a change in the value of the objective function, can then be found through the chain rule

$$\boldsymbol{J}(\boldsymbol{b}) = \frac{\partial \boldsymbol{f}^*(\boldsymbol{b})}{\partial \boldsymbol{b}} = \frac{\partial \boldsymbol{f}(\boldsymbol{z})}{\partial \boldsymbol{z}} \cdot \frac{\partial \boldsymbol{z}(\boldsymbol{q})}{\partial \boldsymbol{q}} \cdot \frac{\partial \boldsymbol{q}(\boldsymbol{b})}{\partial \boldsymbol{b}} \qquad (11)$$

$$\frac{\partial \boldsymbol{f}(\boldsymbol{z})}{\partial \boldsymbol{z}} = \frac{\partial}{\partial \boldsymbol{z}}(\boldsymbol{z} - \boldsymbol{z}^T) = 1 \qquad (12a)$$

$$\frac{\partial \boldsymbol{z}(\boldsymbol{q})}{\partial \boldsymbol{q}} = -\boldsymbol{D}^{-1} \cdot \boldsymbol{C}^t \cdot \boldsymbol{W} \qquad (12b)$$

$$\frac{\partial \boldsymbol{q}(\boldsymbol{b})}{\partial \boldsymbol{b}} = \frac{\partial}{\partial \boldsymbol{b}}(\boldsymbol{K} \cdot \boldsymbol{b}) = \boldsymbol{K} \qquad (12c)$$

$$\boldsymbol{J}(\boldsymbol{b}) = \frac{\partial \boldsymbol{f}^*(\boldsymbol{b})}{\partial \boldsymbol{b}} = -\boldsymbol{D}^{-1} \cdot \boldsymbol{C}^t \cdot \boldsymbol{W} \cdot \boldsymbol{K} \qquad (13)$$

with $\boldsymbol{W} = (\boldsymbol{C}\boldsymbol{z} + \boldsymbol{C}_f \boldsymbol{z}_f)$, the diagonal matrix of the vertical coordinate differences.

3.4 Results

The solving procedure discussed above was implemented in MatLab [18] with $\tau = 10^{-06}$ and $\varepsilon_1 = \varepsilon_2 = 10^{-09}$ for the user-chosen parameters, and with a maximum number of iterations, k_{max}, of 200. The anticlastic target surface, T, is derived from a hyperbolic paraboloid (hypar) that was rotated over 45º and translated over a certain distance in the x, y, and z directions, so that the high points of the surface are at (0,0,1.18) and (1,1,0.46), and the low points at (0,1,0) and (1,0,0).

Figure 5 depicts the target surface T and different 3D tension-only networks at equilibrium with the loads, for different chosen, initial values for the force densities.

The loads are distributed equally over the nodes. The spheres in the middle and left column in Figure 5 represent the vertical difference between each node of the respective equilibrium networks and the corresponding nodes of the target surface; blue spheres depict nodes that lie under the target surface, and orange spheres nodes above it.
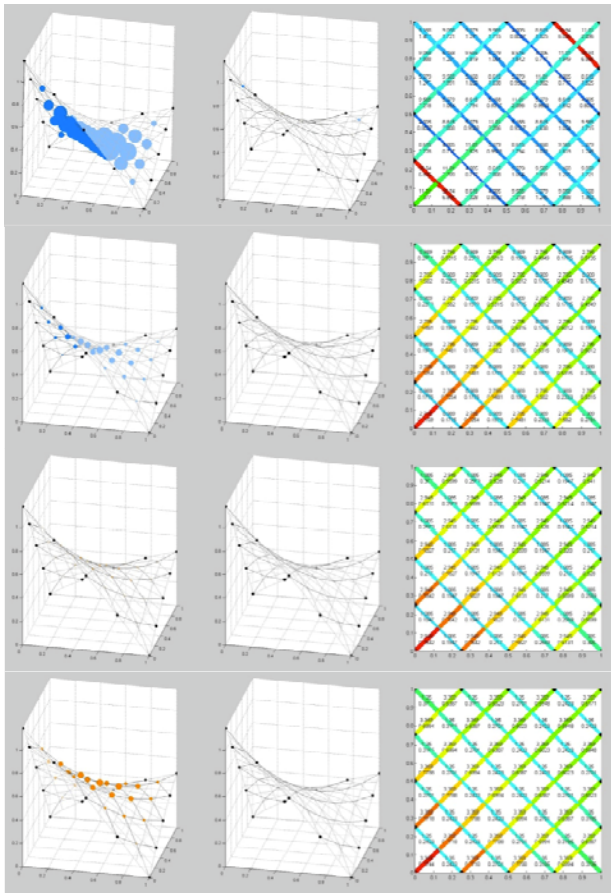
***Figure 5**. (left and middle columns) Target surface, equilibrium network, and z-differences between corresponding nodes, (left) after initial linear form finding, for different chosen values of force densities in the hanging and arching direction (middle) after the optimization process. (right) Distribution of force densities (top number) and resulting branch forces (bottom number) after optimization process.*

***Table 1**. Overview of the results of the optimization process for different starting points (cases). The starting points are the results of linear form finding processes with different chosen values for the force densities in the hanging (q_H) and arching (q_A) directions. k is the number of iterations.*

Case	Before			k	After		
	q		$\sum(z-z^T)^2$		q		$\sum(z-z^T)^2$
	q_A	q_H			q_A	q_H	
1	1	1	0.3099	49	Figure 6		8.89×10^{-04}
2	1	2	0.0287	24	0.989	2.795	8.18×10^{-18}
3	1	3	9.02×10^{-4}	6	1.085	2.945	2.42×10^{-18}
4	1	4	0.0242	22	1.350	3.359	2.08×10^{-16}

Each of the equilibrium networks provides a different starting position for the optimization process. Based on the sum of squared z-differences, case 3 provides the best start, with an initial F-value of 9.02×10^{-04} as seen in Table 1.

A different solution, with different distributions of force densities and thus different distributions of internal forces, is found for each starting position. This indicates that there are several local minima for the cost function, and that additional conditions should be imposed to find a specific local minimum or even a global minimum; for example, conditions on the minimum and/or maximum values of the force densities.

4. CONCLUSIONS

This paper presented a strategy, using an overall optimization process, for finding the closest possible tension-only, equilibrium surface to a given target surface under given loading conditions (i.e. weight of the concrete).

The TNA approach, based on reciprocal diagrams, clarifies the conditions under which the optimization process should be conducted. The LMA approach has been identified as a good procedure for finding an optimized solution. Further refinement of the optimization strategy is possible, as described in [17], for example for more irregular shapes or loading conditions, where the starting position is far from the optimal solution. The TNA-FDM-based form finding procedure furthermore opens possibilities for integrating the procedure into the overall TNA methodology, ultimately leading to the creation of an integrated framework for the simultaneous design of concrete shells and their pre-stressed membrane formwork.

Further extensions of the procedure could lead to form finding approaches for pre-stressed membrane structures in general, where designers have a more intuitive control over the 3D equilibrium shape through the use of reciprocal diagrams.

Future work should be focussed on including additional constraints in the optimization process, e.g. conditions that limit the branch forces to the strength of a specific membrane material, and the building of prototypes.

REFERENCES

[1] *Moreyra Garlock, M., and Billington, D., Felix Candela: Engineer, Builder, Structural Artist.* New Haven and London, Yale University Press, 2009.

[2] *Guldentops, L., Mollaert, M., Adriaenssens, S., De Laet, L., and De Temmerman, N.,* Fabric Formwork for Concrete Shells, *Proceedings of the IASS Symposium 2009*, Valencia, Spain, 2009.

[3] *Ramm, E., Bletzinger, K.-U., and Reitinger, R.,* Shape optimization of shell structures, *Bulletin of the International Association for Shell and Spatial Structures*, Vol. 34, No. 2, 1993, pp. 103-122.

[4] *Tomás, A., and Martí, P.,* Optimality of Candela's Concrete Shells. A Study of His Posthumous Design, *Journal of the International Association for Shell and Spatial Structures*, Vol. 51, No. 1, 2010, pp. 67-77.

[5] *West, M.,* The Center for Architectural Structures and Technology (CAST), http://www.umanitoba.ca/cast_building/.

[6] *Veenendaal, D., Block, P., and West, M.,* History and overview of fabric formwork: Using fabrics for concrete casting, *Structural Concrete*, Vol. 12, No. 3, 2011, pp. 164-177.

[7] *Linkwitz, K., and Schek, H.-J.,* Einige Bemerkungen zur Berechnung von vorgespannten Seilnetzkonstruktionen, *Ingenieur-Archiv*, Vol. 40, 1971, pp. 145-158.

[8] *Schek, H.-J.,* The force density method for form finding and computation of general networks*, Computer Methods in Applied Mechanics and Engineering*, Vol. 3, No. 1, 1974, pp. 115-134.

[9] *Block, P., and Ochsendorf, J.,* Thrust Network Analysis: A new methodology for three-dimensional equilibrium, *Journal of the International Association for Shell and Spatial Structures*, Vol. 48, No. 3, 2007, pp. 167-173.

[10] *Block, P.,* Thrust Network Analysis: Exploring Three-dimensional Equilibrium, PhD dissertation, Massachusetts Institute of Technology, Cambridge, MA, USA, 2009.

[11] *Maxwell, J.C.,* On reciprocal figures and diagrams of forces, *Philosophical Magazine and Journal Series*, Vol. 4, No. 27, 1864, pp. 250-261.

[12] *Ash, P., Bolker, E., Crapo, H., and Whiteley, W.,* Convex polyhedra, Dirichlet tessellations, and spider webs. *Shaping Space: A Polyhedral Approach*, Boston, Birkhäuser, 1988, pp. 231-250.

[13] *Williams, C.J.K.,* Defining and designing curved flexible tensile surface Structures, *The mathematics of surfaces*, 1986, pp. 143-177.

[14] *Block, P., and Lachauer, L.,* Closest-fit, Compression-only Solutions for Free-form Shells, *Proceedings of the IABSE-IASS Symposium 2011*, London, UK, 2011.

[15] *Levenberg, K.,* Method for the solution of certain non-linear problems in least squares, *The Quarterly of Applied Mathematics*, Vol. 2, 1944, pp. 164-168.

[16] *Marquardt, D.,* An algorithm for least-squares estimation of nonlinear parameters, *SIAM Journal on Applied Mathematics*, Vol. 11, 1963, pp. 431-441.

[17] *Madsen, K., Nielsen, H., and Tingleff, O.,* Methods for Nonlinear Least Squares Problems (2nd Ed.), *Informatics and Mathematical Modelling,* Technical University of Denmark, 2004.

[18] The Mathworks MATLAB®: The language of technical computing [Computer software], www.mathworks.com/products/matlab/